Journal of Hazardous Materials 360 (2018) 356–363

Contents lists available at ScienceDirect

Journal of Hazardous Materials

journal homepage: www.elsevier.com/locate/jhazmat

Natural sunlight driven highly efficient photocatalysis for simultaneous degradation of rhodamine B and methyl orange using I/C codoped TiO_2 photocatalyst

Ji-Chao Wang[a,b], Hui-Hui Lou[a], Zhi-Hua Xu[a], Cheng-Xing Cui[a], Zhong-Jun Li[d], Kai Jiang[b], Yu-Ping Zhang[a,*], Ling-Bo Qu[d], Weina Shi[c,*]

[a] College of Chemistry and Chemical Engineering, Henan Institute of Science and Technology, Xinxiang, 453000, China
[b] Post-doctoral Station of Environmental Science and Engineering, Henan Normal University, Xinxiang 453000, China
[c] College of Chemistry and Chemical Engineering, Xinxiang University, Xinxiang 453003, China
[d] College of Chemistry and Molecular Engineering, Zhengzhou University, Zhengzhou 450000, China

GRAPHICAL ABSTRACT

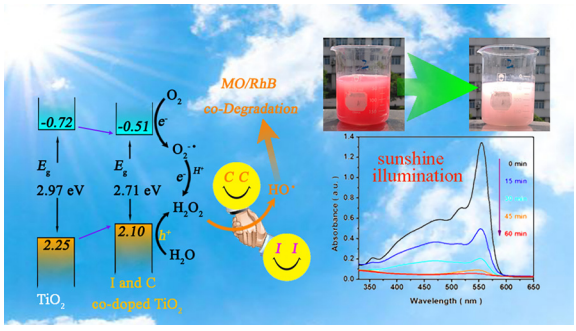

ARTICLE INFO

Keywords:
Photocatalytic degradation
Natural sunlight
Codoping
Hydroxyl radical
H_2O_2

ABSTRACT

Increasing the efficiency of dye degradation is a critical issue for the application for photocatalysis. It is one of the greatest challenges to enhance the utilization of photo generated carriers in semiconductor, especially for sunlight irradiation. In this study, I/C-codoped TiO_2 was synthesized by a simple solvothermal-calcination method. The codoping interstitial carbon and substitutional iodine not only widened the light absorption range of the TiO_2 photocatalysts, but also enhanced the separation of photo-induced carriers. The photocatalytic activities of RhB and MO degradation over the 4-I/C-TiO_2 photocatalyst could reach 98.2% and 94.2% after 25 min visible light irradiation ($\lambda \geq 400$ nm), respectively. Notably, 4-I/C-TiO_2 showed good activity for MO and RhB mixed degradation and could also accomplish the photocatalytic degradation in the above mixed system under natural sunlight irradiation. According to the dark catalytic experiment, I/C-codoping could effectively accelerate the formation of hydroxyl radicals from the generated H_2O_2, which was formed for the enhanced photo-

Abbreviations: RhB, rhodamine B; MO, methyl orange; C-TiO_2, C doped TiO_2; I-TiO_2, I doped TiO_2; I/C-TiO_2, I and C codoped TiO_2; XRD, X-ray diffraction; TEM, Transmission electron microscope; SEM, scanning electron microscope; XPS, X-ray photoelectron spectroscopy; DRS, UV–vis diffuse reflectance spectrum; ESR, electron spin-resonance spectroscopy; VB, valence band; CB, conduction band; P25, commercial TiO_2(Degussa); EDTA-Na, edetate disodiums; t-BuOH, tert-butanol

* Corresponding authors.
E-mail addresses: wangjichao@hist.edu.cn (J.-C. Wang), beijing2008zyp@163.com (Y.-P. Zhang), shiweina516@163.com (W. Shi).

https://doi.org/10.1016/j.jhazmat.2018.08.008
Received 23 May 2018; Received in revised form 20 July 2018; Accepted 4 August 2018
Available online 06 August 2018

catalytic activity of dye degradation. The gained knowledge may provide some insights into the photocatalytic degradation over the codoped TiO_2 catalyst.

1. Introduction

In recent years, the serious environmental problem has become a threat to human survival and development. Among the diverse environmental pollutions, water pollution has become more serious with the rapid industrial development and population growth. An eco-friendly and energy-saving method is thus strongly desired for wastewater treatment. [1] Photocatalytic degradation, as a cheap and environmentally friendly technology, has drawn extensive attention [2]. The photocatalyst plays a key role for high-efficient photocatalysis. TiO_2 has been widely investigated owing to its non-toxicity, low-cost, and good stability property as compared with other materials. [3] However, there are two major barriers for the photocatalytic application of pure TiO_2 [4]. Firstly, TiO_2 has a wide band gap (~3.2 eV for anatase phase), which could only be motivated by the ultraviolet light. [5] Secondly, the rapid recombination of photo-induced carriers results in low efficiency of photocatalytic reactions [6].

To overcome the above problems, various methods such as element doping, [3,7,8] and surface sensitization [9] have been applied to exploring highly active TiO_2 photocatalysts in recent years. In fact, doping TiO_2 with metal or nonmetal elements, as an intelligent strategy, could not only narrow the band gap, but also decrease the required activation energy. Moreover, it is notable that nonmetal element doping is considered to be more environmentally friendly and effective than metal element doping due to its lower thermal stability. Nitrogen, [3] carbon [10], sulfur [11] and iodine [12] are the most widely used species for nonmetal element doping of TiO_2. I-doped TiO_2, which was firstly reported by Hong et al, [13] has shown excellent photocatalytic performance under visible-light irradiation. A substitutional doping introduces localized I 5p orbitals slightly above the semiconductor's valence band, and thus narrowed the band gap of TiO_2 semiconductor. [14] Besides, it is expected that carbon inserted into the lattice of TiO_2 could extend the absorption spectrum into visible region and retard the recombination of photo-excited electrons and holes. [15] In order to increase the doping effectiveness, codoping has been intensively investigated due to its synergistic effects of the both dopants as compared with the single dopant [16–18]. Wang et al. supposed that I and N codoping was beneficial for widening the light absorption range and facilitating the transfer of photo-induced electrons to the surface, leading to improved activity of the photocatalytic degradation [19]. Zhang et al. proved that Sc and C codoped TiO_2 enhanced the photocatalytic performance of Acid orange 7 degradation, which was due to the increased surface area, surface hydroxyl groups, and lifetime of the photo-induced electron-hole pairs. [20] The codoped TiO_2 samples demonstrated improved visible light photo-catalytic activities as compared with the single doped TiO_2 [3,15,20].

Apart from the narrow band-structure of doped TiO_2 photocatalysts, the influence of different surface characteristics induced by the impurity on the formation of surface active substances is never ignored. [1] The generation and transformation of surface active species such as hydroxyl radical (·OH), superoxide radical (O_2^-·), hydrogen peroxide (H_2O_2) and hydroperoxyradical (·OOH) are important for the enhancement of photocatalytic degradation performance. [4] Xu et al. [21] proved that the decomposition of H_2O_2 to ·OH and O_2^-· was promoted with the increased Fe^{3+}/Fe^{2+} ratio on the surface of Ag_3PO_4@$NiFe_2O_4$, leading to higher antibacterial property and photocatalytic activity for methyl orange (MO) degradation. Choi et al. reported that the electron transfer property of TiO_2 was promoted by the modification of surface amino-acids, resulting in efficient peroxymonosulfate production under visible light irradiation. Ortelli et al. [22] found that two process for RhB degradation of de-chromophore and de-ethylation could be driven by ·OH radical on the different TiO_2 surface. Lee et al. [23] proven that, under microwave-assisted UV/TiO_2/PP hybrid process, abundant ·OH radical could be rapidly created, leading to enhance the rate of MO degradation. Yet, Yu et al. [24] considered that, in waste water treatment by nano-sized TiO_2, the competition between the holes of TiO_2 and the ·OH radicals towards decomposing MO depends on the concentration of MO. A direct hole oxidation was processed under high MO concentration, while under low concentration, hydroxyl oxidation competes strongly and might exceed the direct hole oxidation. Hence, the surface active species caused by impurity codoping could influence the photocatalytic process and activity.

We synthesized a series of I and C codoped TiO_2 catalysts by the solvothermal-calcination method. Photocatalytic degradation activities of RhB, MO and mixed dyes (RhB and MO) were investigated using the as-prepared codoped TiO_2 catalysts under visible light irradiation. The influences of C and I codoping on the formation and transfer of hydroxyl radicals for RhB and MO co-degradation were studied, and the photocatalytic mechanism was further proposed.

2. Experimental

2.1. Photocatalyst preparation

All the chemicals were of analytical reagent grade and used without further purification. I and C codoped TiO_2 (I/C-TiO_2) was prepared by a solvethermal-calcination method. In a typical synthesis, a certain amount of HIO_3 was dissolved in 5 mL distilled water, and a mixed solution of 5 mL *n*-amyl alcohol and 35 mL ethanol was added in the above HIO_3 solution to obtain solution A. Meanwhile, 3.404 g titanium butoxide and 10 mL anhydrous ethanol were mixed to obtain solution B, which was added drop-wise into the solution A under vigorous stirring until the formation of a sol solution. The obtained sol was placed into a 100 mL Teflon-lined autoclave at 185 °C for 10 h. After cooling to room temperature, the precursor was washed with deionized water and dried at 60 °C. Subsequent annealing was carried out in Ar at 475 °C for 1 h with activated carbon around the precursor (Fig. S1). The final products were obtained and denoted as *x*-I/C-TiO_2, where *x* represented the I/Ti molar ratio. I doped TiO_2 (I-TiO_2) and C doped TiO_2 (C-TiO_2) were synthesized by the similar procedure without the addition of HIO_3 and *n*-amyl alcohol, respectively. For comparison, the undoped TiO_2 sample was obtained without the addition of HIO_3 and *n*-amyl alcohol. The dopant contents were determined according to the ICP-AES results (Table S1).

2.2. Characterization

X-ray diffraction (XRD) patterns were measured on an X'Pert PRO X-ray powder diffractometer (PANalytical, Netherlands) with Cu-Kα radiation (λ = 1.5418 Å). A scanning electron microscope (SEM, Nova NanoSEM 450, FEI) was used to characterize the morphologies of the obtained samples. Transmission electron microscopy (TEM) images were obtained on a Tecnai G^2 F20 S-TWIN electron microscope. Furthermore, high-resolution transmission electron microscopy (HRTEM) and energy dispersive X-Ray spectroscopy (EDX) were employed. X-ray photoelectron spectroscopy (XPS) and value band XPS were performed on Kratos Axis-Ultra DLD instrument with Al Kα radiation (150 W) and the binding energy was calibrated to the reference C 1 s peak at 284.3 eV. In order to remove any surface contaminants

and characterize the chemical composition underneath the surface, sputtering was done using an Ar^+ ion beam of 2 kV delivering 100 μA of current. [25] UV–vis diffuse reflectance spectrum (DRS) was obtained by a Cary 5000 UV–vis spectrometer (Agilent Technologies, USA) using $BaSO_4$ as a reference. The electron spin resonance (ESR) spectra were recorded using a Bruker EMX-10/12 spectrometer with a 100 kHz magnetic field modulation at a microwave power level of 19.9 mW. In the ESR analysis, DMPO was applied as trapping agent for ·OH. The tests were carried out as follows: 0.1 mmol DMPO and 1 mg catalyst was suspended in deionized water within centrifugal tube (1 mL). Then 40 μL of solution above was injected into the capillary tube (30 μL) and was irradiated for 10 min under visible light (λ > 400 nm). The resulting solution was used to be analyzed.

2.3. Photocatalytic degradation

The photocatalytic activities of RhB and MO degradation over the as-prepared samples were carried out under visible light irradiation at room temperature. The light source was a 300 W Xe arc lamp (CEL-HXF300, Beijing CEAULIGHT Co.) with a cut-off filter of 400 nm. For a typical photocatalytic experiment, 0.05 *g* catalyst was suspended into 100 mL dye aqueous solution (RhB: 20 mg L^{-1} and MO: 20 mg L^{-1}) with constant stirring. Prior to irradiation, the suspension was magnetically stirred in the dark for 1.0 h to ensure the adsorption and desorption equilibrium. The system was adjusted to pH 4.8 with HCl. During irradiation, 5 mL sample was taken out and centrifuged at given intervals. The concentration of RhB and MO were detected through measuring the absorption intensity of the centrifuged aqueous solution at the wavelength of 555 and 465 nm, respectively. Determination of reactive species and photoelectrochemical property has been measured and the detail experiment was shown in supporting information (S1.1 and S1.2). In cycling experiment, the used photocatalyst was centrifugated at 10,000 rpm for 10 min and washed by ethyl alcohol. Then, the powder was obtained after vacuum drying at 40 °C.

The natural sunlight-driven photocatalysis was measured from Jun. 8 to Aug. 2 2017 in our laboratory (N 35°16′58″ E 113°55′49″) in Xinxiang city, Henan province, China. The light intensity could reach 68.2 ~ 89.4 mW/cm^2. In this experiment, 0.05 g catalyst was suspended into 100 mL mixed dye aqueous solution (RhB: 15 mg L^{-1} and MO: 10 mg L^{-1}, pH 4.8) with constant stirring and the other steps were the same as the above photocatalytic experiments.

3. Results and discussion

3.1. XRD analysis

XRD measurements were performed to investigate the influence of I and C doping on the crystal structure. As presented in Fig. 1, single anatase phase (No: 01-071-1169) was evident for each TiO_2-based sample. The peak intensities of the doped TiO_2 samples became lower and the peak widths were also broadened, which was caused by the nanometric crystallites of these samples. [26] In addition, the (1 0 1) and (2 0 0) peaks of C-TiO_2 and I/C-TiO_2 evidently moved in low-angle region compared with those of the undoped TiO_2 sample (Fig. 1b), which may be due to the deformation of crystal structure caused by C doping. [27]

Table 1
Lattice parameters of the as-prepared samples.

	Crystal parameters (Å)				Crystal parameters (Å)		
	a	b*	c		a	b*	c
TiO_2	3.802	3.802	9.611	2-I/C-TiO_2	3.852	3.852	9.661
C-TiO_2	3.806	3.806	9.646	4-I/C-TiO_2	3.851	3.851	9.659
I-TiO_2	3.834	3.834	9.652	6-I/C-TiO_2	3.845	3.845	9.655

* a and b have the same value in a tetragonal unit.

Based on Bragg's Law and the formula for a tetragonal unit cell: $1/(d_{hkl})^2 = (h^2+k^2)/a^2+l^2/c^2$, the lattice parameters of the as-prepared samples were summarized in Table 1. The lattice parameters of I-TiO_2 were a = 3.834 Å (3.802 Å for undoped anatase) and c = 9.652 Å (9.611 Å for undoped anatase), which were slightly greater than those of undoped TiO_2. It was reasonable since the radius of I^{5+} (0.95 Å) is greater than that of Ti^{4+} (0.61 Å), leading to the extension of bond lengths and the expansion of lattice. [28] Additionally, the lattice parameter along the c-axis of C-TiO_2 was increased by about 0.03 Å compared with that of the undoped TiO_2, which was consistent with swelling of the unit cell caused by the interstitial carbon. [29] The lattice parameters of co-doped TiO_2 have been distinctly changed compared with those of the undoped TiO_2. Based on the XRD results, I and C impurities were substitutionally and interstitially doped into TiO_2 structure, respectively.

3.2. SEM and TEM analysis

The morphology of the as-prepared TiO_2 samples were detected by SEM and TEM measurements and the results were shown in Fig. 2. As shown in Fig. 2a, the undoped TiO_2 particles were aggregatively deposited and the lattice fringe of ~0.354 nm (inset of Fig. 2a) is corresponding to the (1 0 1) plane of TiO_2 with anatase phase. The doped TiO_2 samples maintained spherical in shape, as shown in Fig. 2b-2d. The size distributions were analyzed by measuring about 100 nanoparticles based on TEM images using Gatan software. The particle size basically obeyed the logical normal distribution. The average particle sizes of TiO_2, C-TiO_2, I-TiO_2 and 4-I/C-TiO_2 could reach 30.4, 26.8, 46.8 and 15.0 nm, respectively. In particular, the particle size of 4-I/C-TiO_2

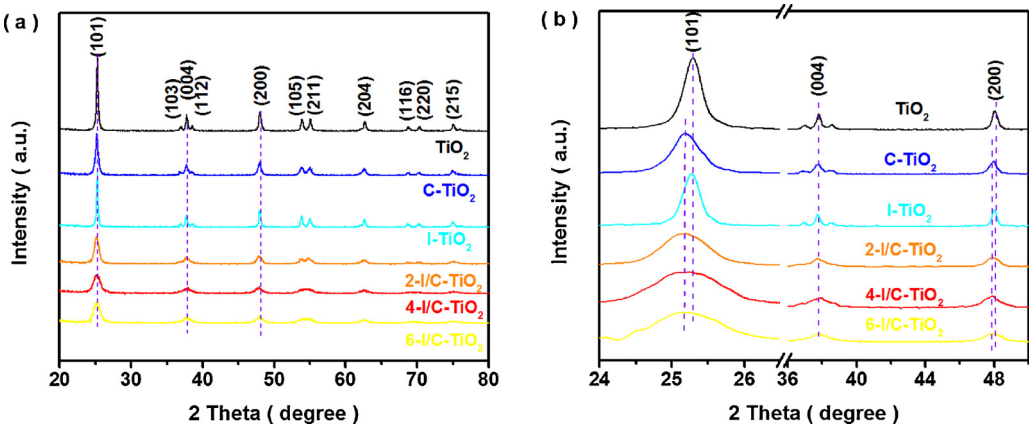

Fig. 1. XRD patterns of the as-prepared TiO_2 based samples (degree range: a. 20–80° and b. 24–49°).

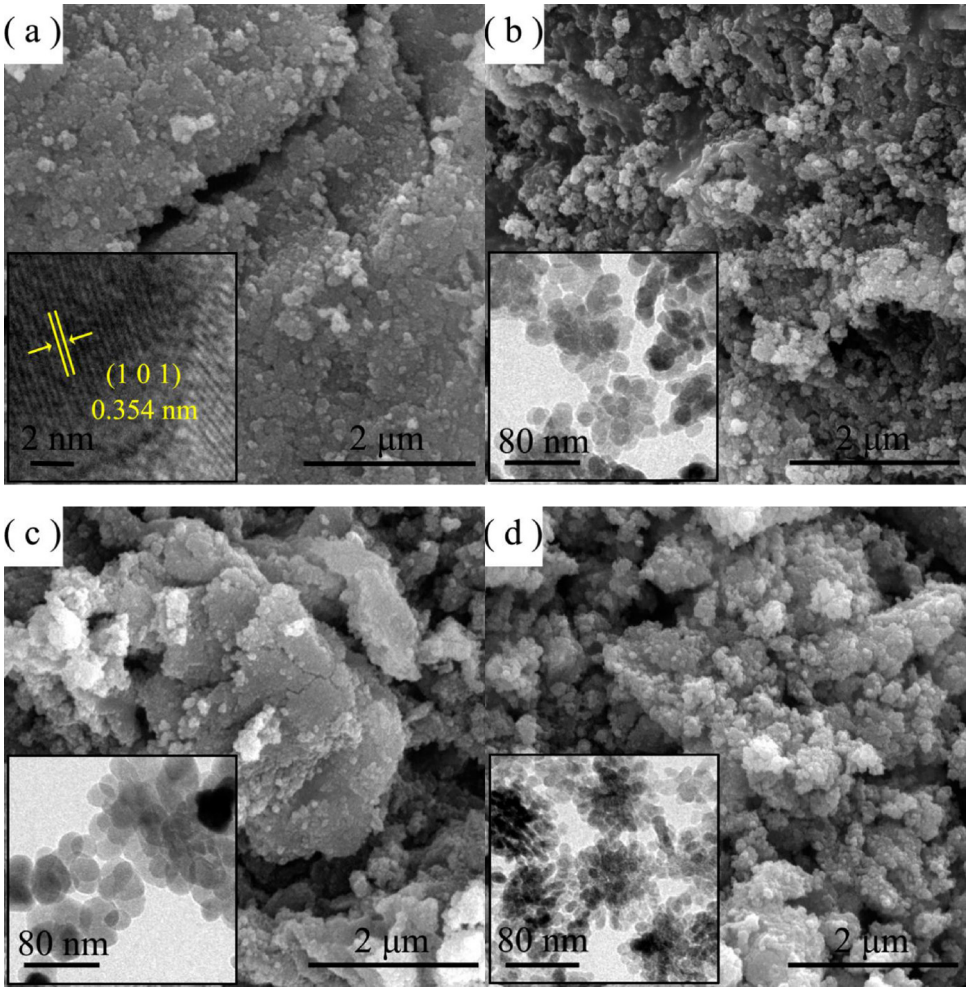

Fig. 2. SEM images of the TiO_2 (a), C-TiO_2 (b), I-TiO_2 (c) and 4-I/C-TiO_2 (d) samples (inset: TEM images of the corresponding samples).

declined evidently as compared with the other samples. According to the N_2 absorption-desorption results (Fig. S2), the surface area of I and C codoped TiO_2 could reach 72.2 m^2/g, which was higher than those of the other samples. It was possible that the crystal structure of TiO_2 deformed due to the doping of impurity ions. Besides, based on the EDX result (Fig. S3), I element was uniformly distributed on the surface of I doped TiO_2, which indicated that I impurity was assuredly doped into the TiO_2 sample.

3.3. XPS analysis

The composition and chemical states of the 4-I/C-TiO_2 sample were analyzed by XPS measurements. Fig. 3a showed the high resolution XPS spectrum of Ti 2p core levels. The characteristic peaks were located at 458.5 and 464.3 eV, corresponding to Ti $2p_{3/2}$ and Ti $2p_{1/2}$, respectively. [30] The splitting energy between the Ti $2p_{1/2}$ and Ti $2p_{3/2}$ peaks was ~5.8 eV, indicating a normal Ti^{4+} state. Moreover, the distinct peak of Ti^{3+} at 456.2 eV also appeared in the 4-I/C-TiO_2 sample. [7] The O1 s spectrum of the 4-I/C-TiO_2 sample was shown in Fig. 3b. As can be seen, the three peaks centered at 529.6, 531.2 and 533.3 eV were attributed to Ti—O—Ti, Ti—O—H and Ti—O—I, respectively. [31,32] Additionally, the I 5d spectrum presented in Fig. 3c confirmed the presence of I^{5+} at 623.6 eV. [33] The C 1 s spectrum in Fig. 3d exhibited three peaks at 288.7, 286.4 and 283.0 eV, corresponding to C═O, C—O and Ti—C—O, respectively. To explore the occupancy sites of the doped impurity in 4-I/C-TiO_2 sample, we used Ar^+ sputtering to remove surface contaminants and studied the chemical composition underneath the surface. In the high resolution spectra of the Ti, I and C elements before and after sputtering (Fig. S4), the sputtering itself created oxygen deficiency leading to the formation of lower oxides, which may cause the transformation from substitutionally placed I to interstitially placed I, [34] and the existence of interstitial C impurity was discovered [25]. Combining with the XRD results, I and C impurities were substitutionally and interstitially doped into the TiO_2 structure, respectively.

3.4. Band structure of photocatalysts

To confirm the band-gap of photocatalysts, the UV–vis diffuse reflectance spectra of the as-prepared TiO_2 samples were obtained and the results were shown in Fig. 4. The absorption edge of pure TiO_2 was around 400 nm, while those of the doped TiO_2 samples exhibited distinctly red shift. The indirect bad gap energies (E_g) of the photocatalysts were calculated by plotting $(\alpha h\nu)^{1/2}$ *vs.* band-energy (inset of Fig. 4) using the Kubelka-Munk theory, [36] which was usually applied to the impurity-doped catalyst [35]. The apparent band gaps of TiO_2, C-TiO_2, I-TiO_2 and 4-I/C-TiO_2 could reach 2.97, 2.89, 2.83 and 2.71 eV, respectively. Besides, it is notable that the absorption in the 620–800 nm light region was distinctly enhanced except for that of the undoped TiO_2 sample, which may be caused by the formation of structure defect or Ti^{3+} [37].

XPS valence band spectra were measured to investigate the effect of I and C doping on the band structures of the photocatalysts. As shown in Fig. S5, the valence band (VB) potential of C-TiO_2 was located at

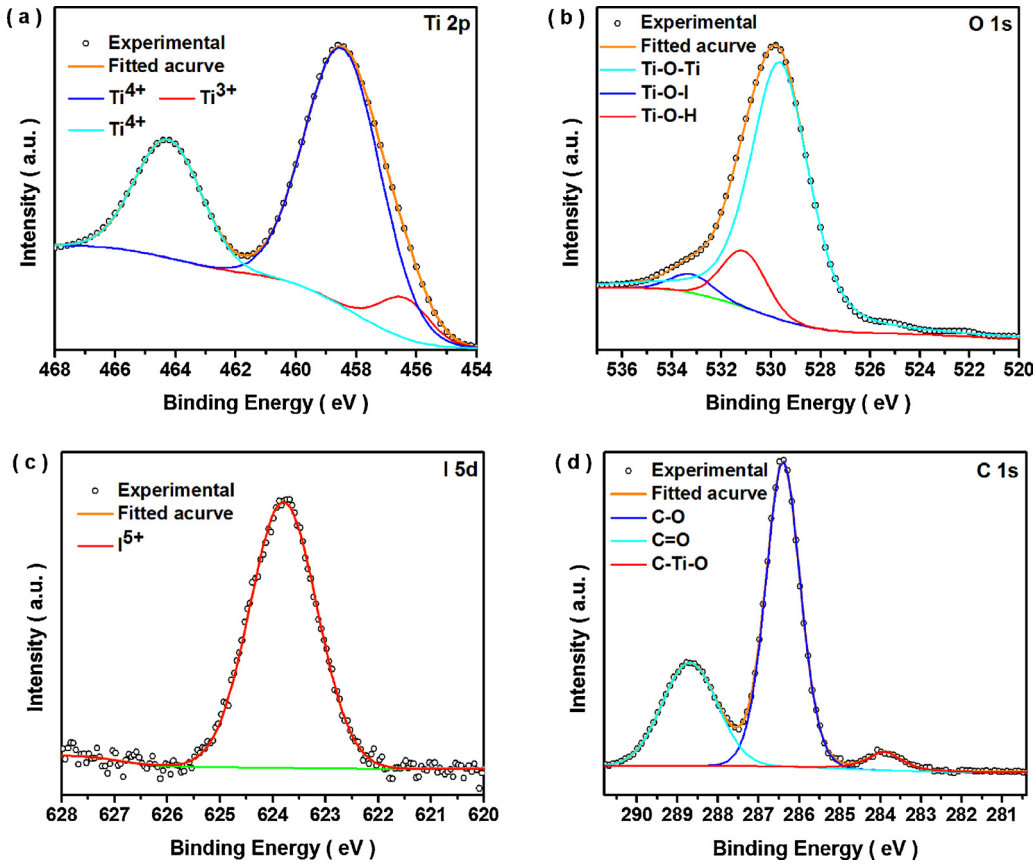

Fig. 3. XPS spectra of the 4-I/C-TiO_2 sample: (a) Ti 2p; (b) O 1 s; (c) I 5d and (d) C 1 s.

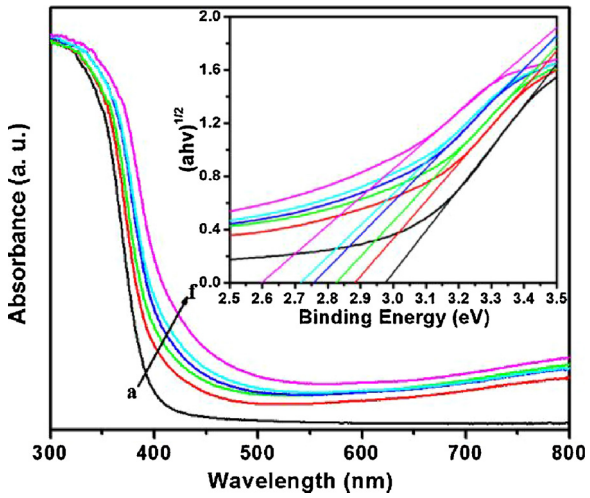

Fig. 4. DRS spectra of the as-prepared TiO_2 photocatalysts (a: TiO_2, b: C-TiO_2, c: I-TiO_2, d: 2-I/C-TiO_2, e: 4-I/C-TiO_2 and f: 6-I/C-TiO_2).

2.21 eV, which was similar with that of the undoped TiO_2 (2.25 eV). Besides, the VB potential of I-TiO_2 shifted toward higher binding energy (2.13 eV), which may be due to that the doped I 5p orbitals with a higher potential lay above the O 2p orbitals and the potential of C 2p orbitals stayed below that of O 2p. [38,39] Combined with the UV–vis absorption results, the conduction band (CB) potential shifted to −0.68 eV for the C-TiO_2 photocatalyst, as shown in Fig. S6. Similarly, the CB and VB potentials of 4-I/C-TiO_2 located at −0.51 and 2.10 eV, respectively.

3.5. Photocatalytic performance

Photocatalytic activities of RhB and MO degradation using the as-prepared photocatalysts were investigated under visible light irradiation ($\lambda \geq 400$ nm). Firstly, control experiments (Fig. S7) confirmed that no appreciable self-decomposition was detected in the absence of either irradiation or photocatalyst. As shown in Fig. 5, after 25 min visible-light irradiation, the degradation efficiency of doped TiO_2 samples all show the better photocatalytic activity of RhB and MO degradation, than that for pristine TiO_2 sample. Especially, 98.6% and 95.3% of RhB and MO dye could be decomposed using 4-I/C-TiO_2 sample, respectively. Yet, beyond 4% iodine content, the photocatalytic activities of codoped TiO_2 distinctly declined, which may result in the formation of recombination center of photoinduced carriers by the excessive impurity atoms. Besides, the photocatalytic activity of 4-I/C-TiO_2 catalysts for RhB and MO degradation still could been beyond 90.0% in the 5th cycling test, as shown in Fig. S8. It suggests that the suitable content of the doped I and C was beneficial for the photocatalytic degradation activity.

To further understand the reaction kinetics of RhB and MO degradation over the photocatalysts, the pseudo-first order model [40] was given by Eq. (1).

$$\ln(c_0/c) = -kt \quad (1)$$

where c_0 and c were the dye concentrations at time 0 and t, respectively, and k is the pseudo-first order rate constant. According to Eq. (1), the pseudo-first order rate constant k was calculated and listed in Table 2. A rather good correlation to the pseudo-first-order reaction kinetics ($R > 0.99$) was found (Fig. S9), and the rate constants increased with I and C doping. The k values of 4-I/C-TiO_2 sample for RhB

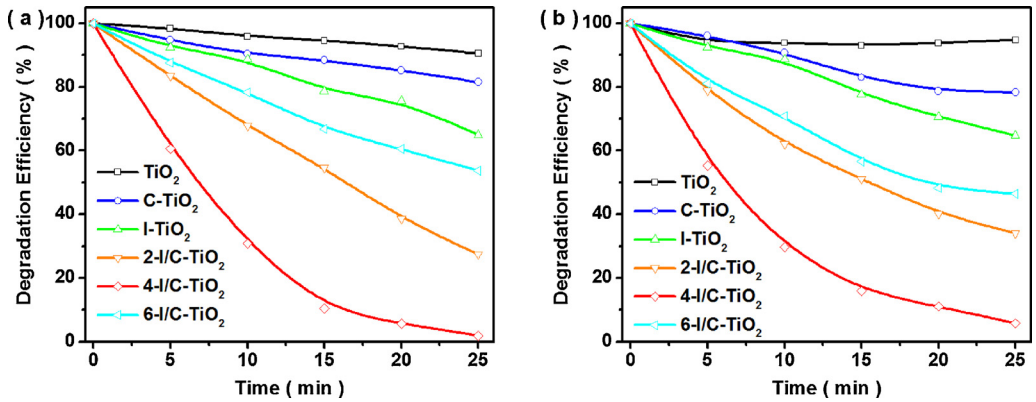

Fig. 5. Photocatalytic activity for RhB (a) and MO (b) degradation using different photocatalysts under visible light irradiation (λ ≥ 400 nm).

Table 2
Degradation rate constants of various photocatalysts for RhB and MO degradation.

	TiO_2	C-TiO_2	I-TiO_2	2-I/C-TiO_2	4-I/C-TiO_2	6-I/C-TiO_2
R_{MO}	0.9936	0.9910	0.9939	0.9988	0.9982	0.9902
k_{MO} (min^{-1})	0.0016	0.0109	0.0177	0.0434	0.1125	0.0321
R_{RhB}	0.9978	0.9937	0.9906	0.9989	0.9935	0.9986
k_{RhB} (min^{-1})	0.0039	0.0078	0.0164	0.0514	0.1600	0.0251

and MO degradation were 0.1600 and 0.1125, which were approximately 70 and 41 times of the pure TiO_2 sample, respectively. The excellent photocatalytic activity of the 4-I/C-TiO_2 could be attributed to the I and C codoping.

Besides, photocatalytic activity of the 4-I/C-TiO_2 sample for the mixed dye degradation was further investigated. As shown in Fig. 6a, the intensities of the characteristic absorption peaks for RhB and MO molecules weakened in the presence of 4-I/C-TiO_2 under Xe lamp irradiation, indicating its excellent photocatalytic activity for the mixed dye degradation, and the activity could maintain well after three cycling tests. Besides, according to the XRD and XPS results (Fig. S10), the crystal structure and chemical compose of 4-I/C-TiO_2 showed no obvious change, indicating its good catalytic stability. Notably, under natural sunlight irradiation for 60 min, the photocatalytic co-degradation for RhB and MO using 4-I/C-TiO_2 could be accomplished, which was evidently higher than that of commercial P25 (Figs. 6b and S11). The 4-I/C-TiO_2 catalyst successfully achieved photocatalytic mixed dye degradation under natural sunlight irradiation.

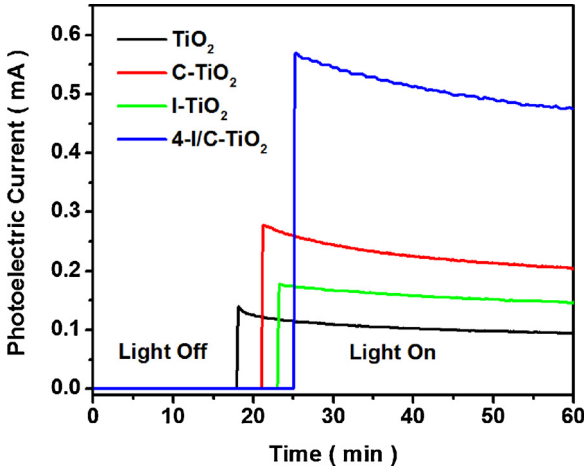

Fig. 7. Photocurrent curves of 4-I/C-TiO_2, C-TiO_2, I-TiO_2 and TiO_2 samples under visible-light illumination.

3.6. Photocatalytic mechanism

Based on the experiment results, the electrons and holes in TiO_2 catalysts could be generated under visible light illumination. Then, the electrons in CB of catalysts should transfer to the TiO_2 surface. The photocurrents of the as-prepared photocatalysts were found under visible-light illumination (Fig. 7).The transient photocurrents of 4-I/C-TiO_2, C-TiO_2 and I-TiO_2 were about 4.9, 2.1 and 1.8 times higher than that of TiO_2, respectively. It was demonstrated that the photo-induced

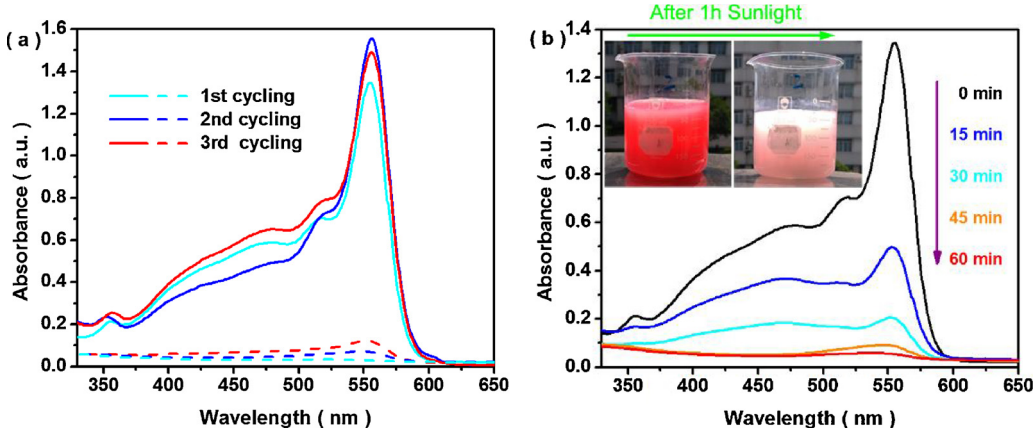

Fig. 6. Photocatalytic activity of the 4-I/C-TiO_2 sample for the mixed dye degradation under Xe lamp irradiation (a. full line and dot line were on behalf of initial and final absorbance, respectively) for 30 min and natural sunlight irradiation (b) for 60 min.

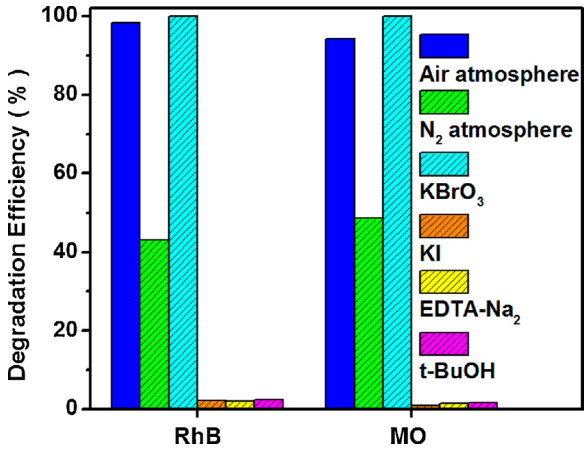

Fig. 8. Photocatalytic activity of RhB or MO degradation under N_2 atmosphere with and without different scavengers.

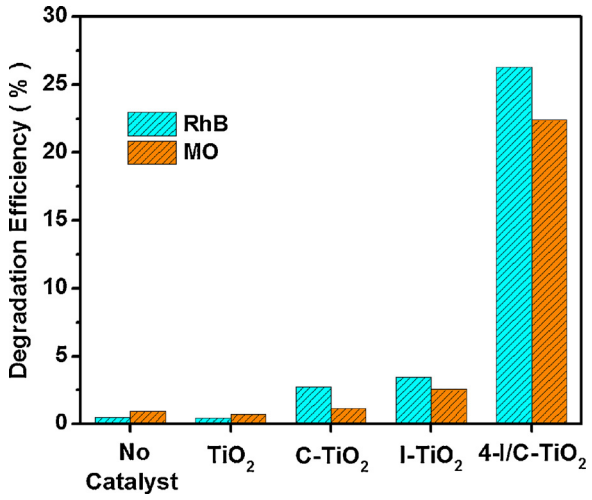

Fig. 10. Catalytic activity of RhB or MO degradation under N_2 atmosphere with 0.1 mL H_2O_2.

carriers could be efficiently separated due to C and I codoping.

Compared with the photocatalytic activity of degradation in N_2 atmosphere (Fig. 8), the existence of dissolved O_2 was benefited for dye degradation. The photocatalytic activity was promoted by adding electron scavenger ($KBrO_3$), and contrary results were obtained with the addition of EDTA-Na (holes scavenger), *t*-BuOH (hydroxide scavenger) and KI (hole and hydroxide scavenger) under N_2 atmosphere, indicating that photogenerated holes and hydroxyl radicals (·OH) played a key role for the photocatalysis of RhB or MO degradation.

Peroxide indicator o-tolidine was added into the catalytic system, and the results in Fig. 9a indicated that H_2O_2 molecules were formed for the catalysts after visible light irradiation for 60 min. According to the intensity of characteristic peak, H_2O_2 contents for the doped TiO_2 samples were higher than that of the undoped TiO_2. Particularly, 4-I/C-TiO_2 didn't show the optimal photocatalytic performance for H_2O_2 production, which may be due to the conversion of H_2O_2 into ·OH. ESR measurements were employed to analyze the formation of ·OH species after 10 min irradiation under N_2 atmosphere (Fig. 9b). An obvious 1:2:2:1 quartet signal was observed for all the catalysts, which was corresponding to the DMPO-·OH adducts. [41] It indicated that the ·OH radicals was generated using TiO_2 sample after light-illumination. The intensity of characteristic peak increased with the existence of the I and C impurity, which implied that doped I and C could promote the ·OH generation. Especially for the 4-I/C-TiO_2 sample, the peak intensity was the strongest among them, indicating the generation of abundant ·OH radicals, and thus leading to high photocatalytic activity.

For further exploring the effect of C and I doping on transform from H_2O_2 to ·OH, the catalytic activities for RhB and MO degradation with the addition of H_2O_2 were tested in the dark for 60 min and the results were illustrated in Fig. 10. As can be seen, 4-I/C-TiO_2 exhibited the best activity for RhB and MO degradation among the catalysts, implying that I and C codoping could be beneficial for the formation of ·OH radicals from H_2O_2 generated on the TiO_2 surface.

Based on the experiment results, the mechanism of RhB/MO degradation is proposed as follows:

$$TiO_2 \rightarrow h_{VB}^{+} + e_{CB}^{-} \quad (2)$$

$$O_2 + e_{CB}^{-} \rightarrow O_2^{-}\cdot \quad (3)$$

$$O_2^{-}\cdot + 2\,H^{+} + e_{CB}^{-} \rightarrow H_2O_2 \quad (4)$$

$$4H_2O + 2\,h_{VB}^{+} \rightarrow H_2O_2 + 2\,H^{+} \quad (5)$$

$$H_2O_2 \rightarrow 2\,\cdot OH \quad (6)$$

$$h_{VB}^{+}/\cdot OH + RhB/MO \rightarrow \text{Degradation Products}^{*} \quad (7)$$

*degradation products including CO_2, NO_3^{-}, H_2O and much micromolecules(detailed in Table S2)

4. Conclusion

I and C codoping TiO_2 was synthesized by a solvothermal-calcination method. The codoping of interstitial carbon and substitutional iodine not only extended the light absorption range of the TiO_2 photocatalysts, but also enhance the separation of photo-induced carriers. The photocatalytic activities of RhB and MO degradation over the 4-I/C-TiO_2 photocatalyst could reach 98.2% and 94.2% after 25 min visible

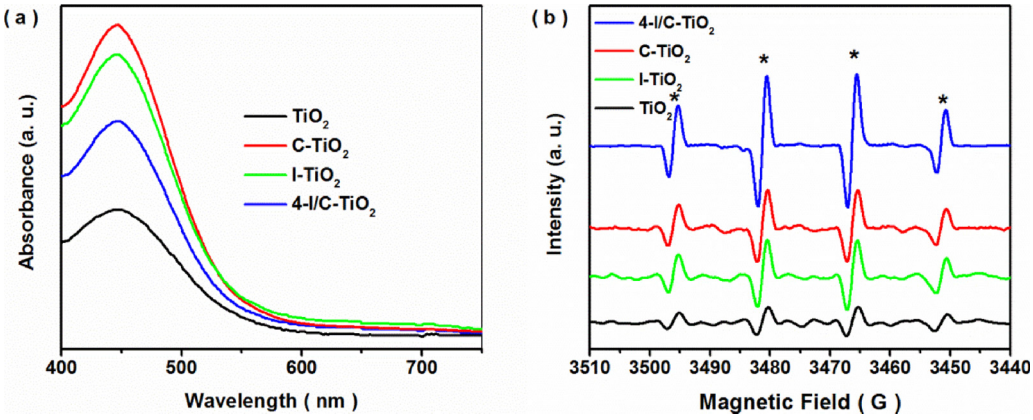

Fig. 9. UV–vis spectra for H_2O_2 capture with o-tolidine (a) and ESR spectra (b) of the 4-I/C-TiO_2, C-TiO_2, I-TiO_2 and TiO_2 samples under light illumination.

light irradiation, respectively. 4-I/C-TiO_2 sample still showed good photocatalytic activity for MO and RhB mixed degradation. Notably, the photocatalytic degradation in the above mixed system could be accomplished using the 4-I/C-TiO_2 under 60 min sunlight irradiation. I and C codoping could effectively accelerate the formation of hydroxyl radicals from the generated H_2O_2, which was formed for the enhanced photocatalytic activity of MO and RhB mixed degradation. Photocatalytic mechanism is finally proposed, and the gained knowledge may provide some insights into the photocatalytic degradation of the mixed-dyes system over the codoped TiO_2 catalyst.

Acknowledgments

This work was supported by National Natural Science Foundation of China (No. 21671059), China Postdoctoral Science Foundation Funded Project (No. 2017M612391), Key Scientific Research Project of Colleges and Universities of Henan Province (No. 18A150027), the Landmark Innovation Project of Henan Institute of Science and Technology (No. 2015BZ02), Key Scientific and Technological Project of Henan Province (182102311084), Henan Postdoctoral Science Foundation, Research Foundation for Advanced Talents of Henan Institute of Science and Technology (No. 2016035) and the Innovation Team in Henan Province (No. C20150020).

Appendix A. Supplementary data

Supplementary material related to this article can be found, in the online version, at doi:https://doi.org/10.1016/j.jhazmat.2018.08.008.

References

[1] M. Cheng, G. Zeng, D. Huang, C. Lai, P. Xu, C. Zhang, Y. Liu, Hydroxyl radicals based advanced oxidation processes (AOPs) for remediation of soils contaminated with organic compounds: a review, Chem. Eng. J. 284 (2016) 582–598.
[2] D. Spasiano, R. Marotta, S. Malato, P. Fernandez-Ibañez, I. Di Somma, Solar photocatalysis: materials, reactors, some commercial, and pre-industrialized applications. A comprehensive approach, Appl. Catal. B: Environ. 170-171 (2015) 90–123.
[3] S.A. Ansari, M.M. Khan, M.O. Ansari, M.H. Cho, Nitrogen-doped titanium dioxide (N-doped TiO_2) for visible light photocatalysis, New J. Chem. 40 (2016) 3000–3009.
[4] Z. Xing, J. Zhang, J. Cui, J. Yin, T. Zhao, J. Kuang, Z. Xiu, N. Wan, W. Zhou, Recent advances in floating TiO_2 -based photocatalysts for environmental application, Appl. Catal. B: Environ. 225 (2018) 452–467.
[5] Z. Zhou, Y. Yu, Z. Ding, M. Zuo, C. Jing, Modulating high-index facets on anatase TiO_2, Eur. J. Inorg. Chem. 2018 (2018) 683–693.
[6] L. Xiang, X. Zhao, Wet-chemical preparation of TiO_2-Based composites with different morphologies and photocatalytic properties, Nanomaterials 7 (2017) 310.
[7] Y. Cao, Z. Xing, Y. Shen, Z. Li, X. Wu, X. Yan, J. Zou, S. Yang, W. Zhou, Mesoporous black Ti^{3+} /N-TiO_2 spheres for efficient visible-light-driven photocatalytic performance, Chem. Eng. J. 325 (2017) 199–207.
[8] J. Liu, L. Han, N. An, L. Xing, H. Ma, L. Cheng, J. Yang, Q. Zhang, Enhanced visible-light photocatalytic activity of carbonate-doped anatase TiO_2 based on the electron-withdrawing bidentate carboxylate linkage, Appl. Catal. B: Environ. 202 (2017) 642–652.
[9] M. Karakus, W. Zhang, H.J. Rader, M. Bonn, E. Canovas, Electron transfer from Bi-isonicotinic acid emerges upon photodegradation of N3-sensitized TiO_2 electrodes, ACS. Appl. Mater. Interface 9 (2017) 35376–35382.
[10] J. Shao, W. Sheng, M. Wang, S. Li, J. Chen, Y. Zhang, S. Cao, In situ synthesis of carbon-doped TiO_2 single-crystal nanorods with a remarkably photocatalytic efficiency, Appl. Catal. B: Environ. 209 (2017) 311–319.
[11] X. Yan, K. Yuan, N. Lu, H. Xu, S. Zhang, N. Takeuchi, H. Kobayashi, R. Li, The interplay of sulfur doping and surface hydroxyl in band gap engineering: mesoporous sulfur-doped TiO_2 coupled with magnetite as a recyclable, efficient, visible light active photocatalyst for water purification, Appl. Catal. B: Environ. 218 (2017) 20–31.
[12] H. Lin, W. Deng, T. Zhou, S. Ning, J. Long, X. Wang, Iodine-modified nanocrystalline titania for photo-catalytic antibacterial application under visible light illumination, Appl. Catal. B: Environ. 176-177 (2015) 36–43.
[13] X. Hong, Z. Wang, W. Cai, F. Lu, J. Zhang, Y. Yang, N. Ma, Y. Liu, Visible-light-Activated nanoparticle photocatalyst of iodine-doped titanium dioxide, Chem. Mater. 17 (2005) 1548–1552.
[14] R. Long, Y. Dai, B. Huang, Structural and electronic properties of iodine-doped anatase and rutile TiO_2, Comp. Mater. Sci. 45 (2009) 223–228.
[15] I.V. Baklanova, V.P. Zhukov, V.N. Krasil'nikov, O.I. Gyrdasova, L.Y. Buldakova, E.V. Shalaeva, E.V. Polyakov, M.V. Kuznetsov, I.R. Shein, E.G. Vovkotrub, Fe and C doped TiO_2 with different aggregate architecture: synthesis, optical, spectral and photocatalytic properties, first-principle calculation, J. Phys. Chem. Solids 111 (2017) 473–486.
[16] J. Yu, P. Zhou, Q. Li, New insight into the enhanced visible-light photocatalytic activities of B-, C- and B/C-doped anatase TiO_2 by first-principles, Phys. Chem. Chem. Phys. 15 (2013) 12040–12047.
[17] L. Liao, C.W. Ingram, Mesoporous I-Ag codoped titania and alumina modified titania catalysts: synthesis, characterization and photocatalytic properties, Appl. Catal. A: Gene 433-434 (2012) 18–25.
[18] X. Yan, Z. Xing, Y. Cao, M. Hu, Z. Li, X. Wu, Q. Zhu, S. Yang, W. Zhou, In-situ C-N-S-tridoped single crystal black TiO_2 nanosheets with exposed {001} facets as efficient visible-light-driven photocatalysts, Appl. Catal. B: Environ. 219 (2017) 572–579.
[19] X. Wang, J. Song, J. Huang, J. Zhang, X. Wang, R. Ma, J. Wang, J. Zhao, Activated carbon-based magnetic TiO_2 photocatalyst codoped with iodine and nitrogen for organic pollution degradation, Appl. Surf. Sci. 390 (2016) 190–201.
[20] M. Nasir, J. Lei, W. Iqbal, J. Zhang, Study of synergistic effect of Sc and C codoping on the enhancement of visible light photo-catalytic activity of TiO_2, Appl. Surf. Sci. 364 (2016) 446–454.
[21] S. Huang, Y. Xu, T. Zhou, M. Xie, Y. Ma, Q. Liu, L. Jing, H. Xu, H. Li, Constructing magnetic catalysts with in-situ solid-liquid interfacial photo-Fenton-like reaction over Ag_3PO_4 @$NiFe_2O_4$ composites, Appl. Catal. B: Environ. 225 (2018) 40–50.
[22] S. Ortelli, M. Blosi, S. Albonetti, A. Vaccari, M. Dondia, A.L. Costa, TiO_2 based nano-photocatalysis immobilized on cellulose substrates, J. Photochem. Photobio. A: Chem. 276 (2013) 58–64.
[23] H. Lee, Y.-K. Park, S.-J. Kim, B.-H. Kim, H.-S. Yoon, S.-C. Jung, Rapid degradation of methyl orange using hybrid advanced oxidation process and its synergistic effect, J. Industrial Eng. Chem. 35 (2016) 205–210.
[24] L. Yu, J. Xi, M.-D. Li, H.T. Chan, T. Su, D.L. Phillips, W.K. Chan, The degradation mechanism of methyl orange under photo-catalysis of TiO_2, Phys. Chem. Chem. Phys. 14 (2012) 3589–3595.
[25] A. Chatzitakis, M. Grandcolas, K. Xu, S. Mei, J. Yang, I.J.T. Jensen, C. Simon, T. Norby, Assessing the photoelectrochemical properties of C, N, F codoped TiO_2 nanotubes of different lengths, Catal. Today 287 (2017) 161–168.
[26] M. Blosi, S. Albonetti, S. Ortelli, A.L. Costa, L. Ortolanic, M. Dondia, Green and easily scalable microwave synthesis of noble metal nanosols (Au, Ag, Cu, Pd) usable as catalysts, New J. Chem. 38 (2014) 1401–1409.
[27] X. Yang, C. Cao, K. Hohn, L. Erickson, R. Maghirang, D. Hamal, K. Klabunde, Highly visible-light active C- and V-doped TiO_2 for degradation of acetaldehyde, J. Catal. 252 (2007) 296–302.
[28] J. He, Q. Liu, Z. Sun, W. Yan, G. Zhang, Z. Qi, P. Xu, Z. Wu, S. Wei, High photocatalytic activity of rutile TiO_2 induced by iodine doping, J. Phys. Chem. C 114 (2010) 6035–6038.
[29] N. Feng, A. Zheng, Q. Wang, P. Ren, X. Gao, S.-B. Liu, Z. Shen, T. Chen, F. Deng, Boron environments in B-doped and (B, N)-codoped TiO_2 photocatalysts: a combined solid-state NMR and theoretical calculation study, J. Phys. Chem. C 115 (2011) 2709–2719.
[30] C. Yang, X. Wei, J. Hao, Colossal permittivity in TiO_2 codoped by donor Nb and isovalent Zr, J. Am. Ceram. Soc. 101 (2018) 307–315.
[31] Y. Wang, J. Ren, G. Liu, P. Peng, Synthesis and characterization of iodine ion doped mesoporous TiO_2 by sol–gel method, Mater. Chem. Phys. 130 (2011) 493–499.
[32] W. Deng, S. Ning, Q. Lin, H. Zhang, T. Zhou, H. Lin, J. Long, Q. Lin, X. Wang, I-TiO_2/PVC film with highly photocatalytic antibacterial activity under visible light, Colloids Surf. B Biointerfaces 144 (2016) 196–202.
[33] Q. Zhang, Y. Li, E.A. Ackerman, M. Gajdardziska-Josifovska, H. Li, Visible light responsive iodine-doped TiO_2 for photocatalytic reduction of CO_2 to fuels, Appl. Catal. A Gen. 400 (2011) 195–202.
[34] S. Hashimoto, A. Tanaka, Alteration of Ti 2p XPS spectrum for titanium oxide by low-energy Ar ion bombardment, Surf. Interface Anal. 34 (2002) 262–265.
[35] W. Li, R. Liang, A. Hu, Z. Huang, Y.N. Zhou, Generation of oxygen vacancies in visible light activated one-dimensional iodine TiO_2 photocatalysts, RSC Adv. 4 (2014) 36959–36966.
[36] S. Ortelli, C. Poland, G. Baldi, A.L. Costa, Silica matrix encapsulation as a strategy to control ROS production while preserving photoreactivity in nano-TiO_2, Environ. Sci. Nano 3 (2016) 602–610.
[37] W. Dong, H. Li, J. Xi, J. Mu, Y. Huang, Z. Ji, X. Wu, Reduced TiO_2 nanoflower structured photoanodes for superior photoelectrochemical water splitting, J. Alloys 724 (2017) 280–286.
[38] J. Hwang, S.S. Kalanur, H. Seo, Identification of visible photocatalytic and photoelectrochemical properties of I-TiO_2 via electronic band structure, Electrochim. Acta 252 (2017) 482–489.
[39] Y. Lin, S. Zhu, Z. Jiang, X. Hu, X. Zhang, H. Zhu, J. Fan, T. Mei, G. Zhang, Electronic and optical properties of S/I-codoped anatase TiO_2 from ab initio calculations, Solid State Commun. 171 (2013) 17–21.
[40] Y. Li, J. Wang, H. Yao, L. Dang, Z. Li, Chemical etching preparation of BiOI/Bi_2O_3 heterostructures with enhanced photocatalytic activities, Catal. Commun. 12 (2011) 660–664.
[41] J.-C. Wang, J. Ren, H.-C. Yao, L. Zhang, J.-S. Wang, S.-Q. Zang, L.-F. Han, Z.-J. Li, Synergistic photocatalysis of Cr(VI) reduction and 4-Chlorophenol degradation over hydroxylated α-Fe_2O_3 under visible light irradiation, J. Hazard. Mater. 311 (2016) 11–19.